Dispersed Ni nanoparticles stabilize silicon photoanodes for efficient and inexpensive sunlight-assisted water oxidation

Gabriel Loget, Bruno Fabre, Stephanie Fryars, Cristelle Mériadec, Soraya Ababou-Girard

Dispersed Ni Nanoparticles Stabilize Silicon Photoanodes for Efficient and Inexpensive Sunlight-Assisted Water Oxidation

Gabriel Loget,[*,†] *Bruno Fabre,*[†] *Stéphanie Fryars,*[†] *Cristelle Meriadec,*[‡] *and Soraya Ababou-Girard*[‡]

[†] Institut des Sciences Chimiques de Rennes, UMR 6226 CNRS, Matière Condensée et Systèmes Electroactifs (MaCSE), and

[‡] Institut de Physique de Rennes, UMR 6251 CNRS, Equipe de Physique des Surfaces et Interfaces, Université de Rennes 1, Campus de Beaulieu, 35042 Rennes Cedex, France

Corresponding Author

* gabriel.loget@univ-rennes1.fr

ABSTRACT

Ni, electrodeposited on *n*-type Si from aqueous solutions, in the form of isolated or coalescent nanoparticles (NPs) protects the underlying and partially exposed Si from photocorrosion-induced electrical passivation. Such photoanodes, fabricated without the need of additional protecting layers, buried junction and high vacuum techniques, show a high photovoltage of ≈500 mV for the oxygen evolution reaction (OER), state-of-the-art photocurrents and faradaic efficiencies >90 % under AM 1.5G illumination conditions at pH 14. Remarkably, these photoelectrodes are stable and can be operated at the light-limited catalytic current from 10 h to more than 40 h in 1 M NaOH. These findings demonstrate that robust and efficient Si-based photoanodes can be produced easily, which opens new opportunities for the implementation of low-cost Si-based monolithic photoelectrochemical cells for efficient solar fuel production.

TOC GRAPHICS

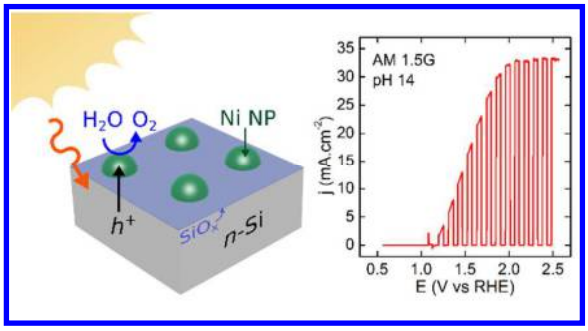

Carbon-free chemical fuels that can be produced from renewable sources are highly promising energy vectors, essential for the development of a sustainable energy economy.[1] In this frame, H_2 is of particular interest because it provides a high energy density, it can be easily stored, transported and readily used to power electrical devices. Alike photosynthesis, where photons are converted into energy-rich molecules, sunlight energy can be converted in H_2 and O_2 using photoelectrochemical water splitting cells (PECs), that are currently attracting tremendous research efforts.[2-7] Monolithic PECs are generally composed of a *p*-type semiconductor (*p*-SC) and an *n*-type SC (*n*-SC) that are in intimate contact and immersed in an aqueous solution. Upon sunlight absorption, photogenerated charge carriers are driven to the solid-liquid interface where they react with water.[2-7] Electrons generated in the *p*-SC reduce water to H_2 while holes, generated in the *n*-SC, oxidize water to O_2 simultaneously. Silicon is considered as one of the most attractive materials for manufacturing PEC photoelectrodes because of its abundance and its wide use in microelectronic and photovoltaic industries.[8] Moreover, it conveniently has a high carrier mobility, a suitable electronic structure and an optimal band gap that allows absorbing all the solar spectrum.[8] Nevertheless, using Si as a photoanode material is very challenging mainly because of two reasons: *i*) water oxidation is a four-electron process, which is sluggish at Si surface and requires a substantial overpotential to occur and *ii*) Si is highly prone to photocorrosion, and its oxidation to insulating SiO_x is the main process arising under anodic polarization.[8-10] The latter phenomenon is strongly pronounced in alkaline media, and induces the quasi-spontaneous passivation of Si photoanodes when used for water splitting. This technological issue had remained a deadlock for the development of Si monolithic PECs for the last decades. Recently, tremendous progress has been made by employing thin film deposition techniques such as physical vapor deposition (PVD) and atomic layer deposition (ALD) for

coating Si with conformal single or multiple thin films that serve as protecting and/or catalytic layers.[8-11] Ni and NiO_x are excellent coating materials as they provide corrosion resistance and a high catalytic activity for the oxygen evolution reaction (OER) at high pH (see table S1).[12,13] In particular, Kenney *et al.* have firstly reported that e-beam evaporated thin Ni layers protect Si photoanodes.[14] Following this work, Ni-based alloys and oxides, sputtered on *n*-Si[15] and np^+-Si[16-18] junctions have demonstrated high performances for OER. Notably, Lewis' team has demonstrated that layers of Ni[19] and $NiCrO_x$,[20] sputtered on TiO_2-protected planar and microstructured np^+-Si junctions, were stable for periods of 100 h[19] and 2200 h,[20] respectively, in strongly alkaline media. Furthermore, a reactive sputter method has been developed for coating Si surfaces with transparent NiO_x layers,[21] that protect Si-based photoelectrodes for prolonged water splitting.[22] If these works constitute major breakthroughs for the implementation of efficient and stable Si-based PECs, they all share the use of high vacuum techniques for the layer deposition. Alternatives to sputtering and ALD would be interesting from a financial point of view but also because they would open exciting possibilities in terms of layer composition and morphologies. In this context, NiO_x layers, deposited by a sol-gel method on *n*-Si have a catalytic activity towards OER at neutral[23] and alkaline pH.[24] Although electrodeposition has been not much explored for this application so far, it is very attractive since it can be easily implemented and it allows a precise control over the coating morphology. In this context, Nocera *et al.* have reported the use of electrodeposited Co-based catalysts, operating at neutral pH on Si.[25] Lately, Switzer's group has shown that inhomogeneous Co particles, electrodeposited on *n*-Si surfaces allow to perform OER for 2 h at high pH and it has been very recently reported that NiFe electrodeposited on np^+-Si is highly effective for OER.[27] High interest is currently being given to the understanding of Si interfaces coated with inhomogeneous co-catalysts layers. In

particular, recent reports have shown that the photovoltages of these photoanodes are independent of the solution potential and suggested that the large barrier heights are caused by the presence of a native SiO_x layer and the inhomogeneous nature of the metal-insulator-semiconductor (MIS) structure that enhance the barrier height.[27,28] However, Ni electrodeposition on *n*-Si was not employed so far to yield efficient photoanodes. In this work, we use electrodeposition to decorate *n*-Si surfaces with Ni co-catalysts and we demonstrate that this method allows to fabricate robust photoanodes for efficient photoelectrochemical water splitting.

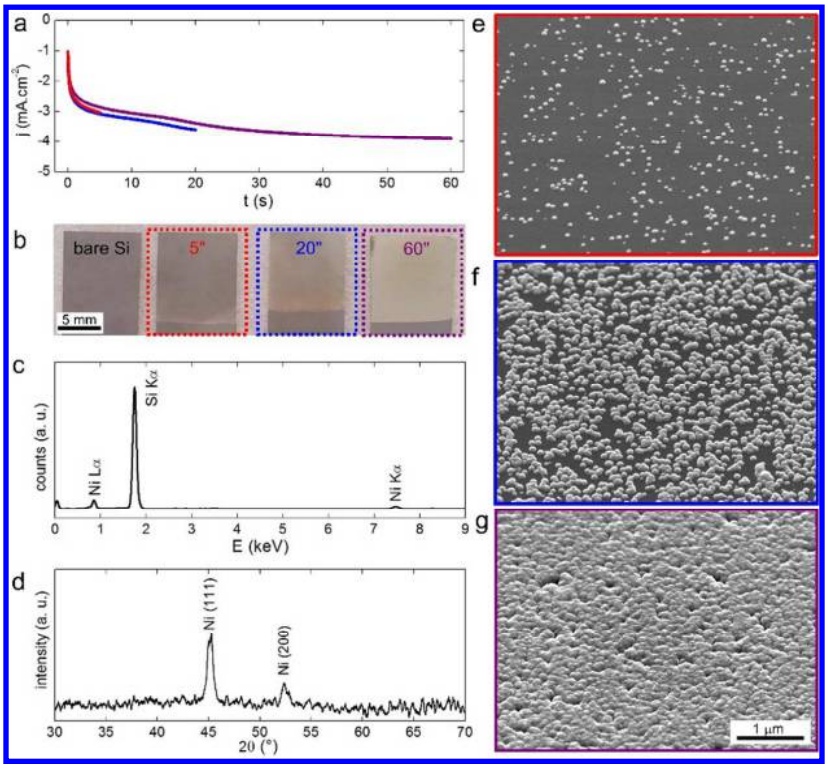

Figure 1. Characterization of the Ni-decorated surfaces. a) Chronoamperograms for Ni electrodeposition on hydrogenated *n*-Si. b) Photographs of bare and Ni-coated *n*-Si. c) EDS and d) XRD spectra of Ni-coated *n*-Si. e-g) SEM pictures showing the Ni deposits on *n*-Si (the

surfaces were tilted by 45°). In these panels, data depicted or framed in red, blue and purple correspond to the surfaces obtained for electrodeposition times of 5 s, 20 s and 60 s, respectively.

In this work, Ni was deposited at -1.5 V vs KCl-saturated calomel electrode (SCE) on freshly hydrogenated *n*-Si (100) from an aqueous solution containing Ni chloride and boric acid. The potentiostatic method allows to conveniently control the amount of deposited material as well as the morphology of the layer over time. Indeed, the chronoamperograms of Fig. 1a reveal the evolution of the electrodeposition kinetics and show that the current density *j* decreased sharply before stabilizing. This is consistent with the formation of nuclei that grow and reach coalescence. The resulting coatings were homogeneous and could be observed with the naked eye (Fig. 1b). Energy-dispersive X-ray spectroscopy (EDS) and X-ray diffraction (XRD) measurements confirmed the presence of crystalline Ni on Si (Fig. 1c and 1d). Scanning electron microscopy (SEM) images, shown in Fig. 1e-g (and Fig S1-3) indicated that 5 s electrodeposition led to a film of randomly-dispersed Ni nanoparticles (Ni NPs) having a mean diameter of 59 ±17 nm (Fig. S4). At 20 s, the Ni NPs grew further and the majority started to merge, creating NP aggregates having a projected area in the range of 0.05 μm², while at 60 s they all coalesced, yielding a deposit that can be considered as a film with a thickness of 68 ±11 nm (Fig. S1d).The photoelectrochemical performances of the so-fabricated surfaces were then tested in 1 M NaOH (measured pH = 14), using simulated sunlight (AM 1.5G, 100 mW cm^{-2}). First, we verified by cyclic voltammetry (CV) that uncoated *n*-Si quickly passivated under these experimental conditions, due to photocorrosion (Fig. S5). Before any experiments, the Ni-coated photoelectrodes were cycled by performing several CV scans under illumination (typically, < 40) until they reached a stable photocurrent curve (see Supporting Information and Fig. S8). Fig. 2 shows the CVs obtained for the coated Si surfaces, under illumination for *n*-Si and in the dark for

n- and p^{++}-Si (note that the potential scale versus reversible hydrogen electrode (RHE), is plotted on the top of Fig. 2). In this work, unless specified, the cell resistance was intentionally uncompensated. In the dark, all currents were negligible (in the range of 1 μA cm^{-2}), except for Ni-coated p^{++}-Si that is essentially behaving as a metal. In contrast, photocurrents densities in the mA cm^{-2} range were measured for Ni-coated *n*-Si under illumination.

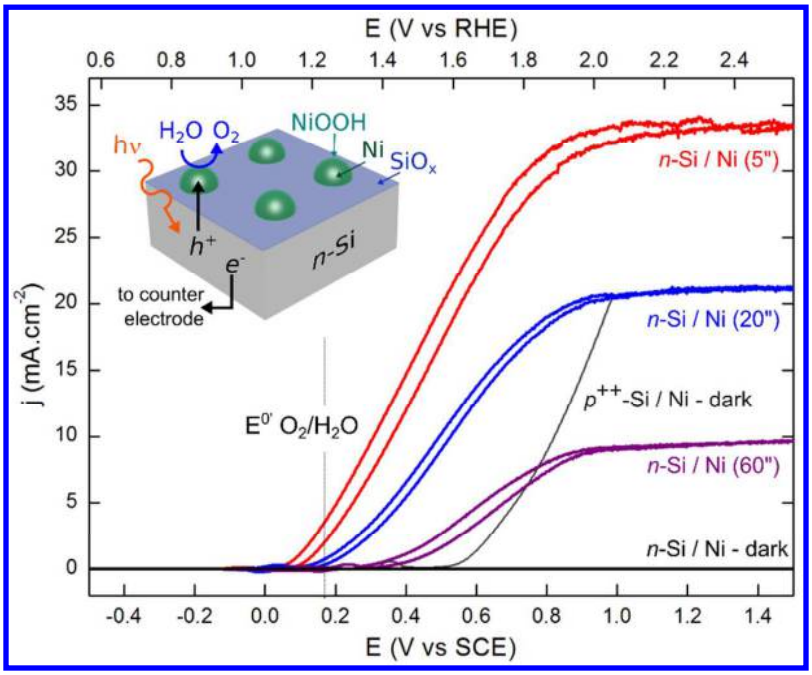

Figure 2. Photoelectrochemical water oxidation. CVs measured in the dark for *n*-Si decorated with Ni NPs (thick black line) and p^{++}-Si coated with Ni (thin black line) and under illumination (AM 1.5G, 100 mW cm^{-2}) for *n*-Si coated with Ni for 5 s (red line), 20 s (blue line) and 60 s (purple line); all the curves were recorded in 1 M NaOH at a sweep rate of 20 mV s^{-1}. Inset: scheme of the surface under illumination.

In all cases, a scan rate-dependent reversible redox wave (Ni^{3+}/Ni^{2+}) was first observed, corresponding to the oxidation of Ni hydroxide to NiOOH (Fig. S6 and Fig. S11), generated at the Ni NP-electrolyte interface upon immersion in the alkaline solution and during the

electrochemical cycling (note that NiOOH is the catalytically active species for OER).[12,29] The determination of the charge under the oxidation peak (shown in Fig. S11 for an electrodeposition time of 5 s), as compared with the NP density and average diameter (Fig. S4), allowed to estimate that about one fifth of the Ni atoms were catalytically-active. This wave was followed, at potential ~100 mV more positive than its cathodic peak (E_{pc}), by the much larger OER photocurrent. Table S2 gathers the photoelectrochemical parameters as a function of the doping type and the Ni amount. From these data, it can be clearly observed that every *n*-Si photoanode exhibited a negative shift of onset potential with respect to the Ni-coated p^{++}-Si anode. The photovoltage and the maximum photocurrent density j_{max} were clearly Ni-dependent and increased with a decreasing amount of electrodeposited Ni. As it can be seen in Fig. 2 and Fig S15, the decoration with isolated Ni NPs (Fig. 1e) provided the highest photovoltage and photocurrent density. This photovoltage of 0.5 V is very close to the one reported for conformal ultrathin Ni coatings prepared by e-beam evaporation on *n*-Si photoanodes without buried junctions.[14] The photocurrent of 33 mA cm^{-2} is in the same range than the one obtained for sputtered Ni-based coatings on np^{+}-Si junctions[21,22] and electrodeposited Co on *n*-Si at comparable pH.[26] The flatband potentials (E_{fb}) were comprised between -0.55 and -0.60 V vs SCE (Fig S7), which is also in good agreement with the values reported for sputtered Ni films.[14] The best electrode generated a photocurrent density of 3.5 mA cm^{-2} at the O_2/H_2O formal potential, corresponding to 16.5 mA cm^{-2} when the cell resistance was compensated, as shown in Fig. S16. The stability of the photoanodes was then evaluated by chronoamperometry (CA) at +1 V vs SCE in the same conditions during a prolonged time. Fig. 3a shows the photocurrent evolution over time for the three different coatings. First, we note that all photocurrents obtained in these experiments were very close to those previously observed in the CVs of Fig. 2. All the

photoanodes maintained at least 70 % of their initial j_{max} over periods longer than 10 h, which is much higher than the durations previously reported at this pH for coatings electrodeposited on *n*-Si surfaces (Table S1).[25,26]

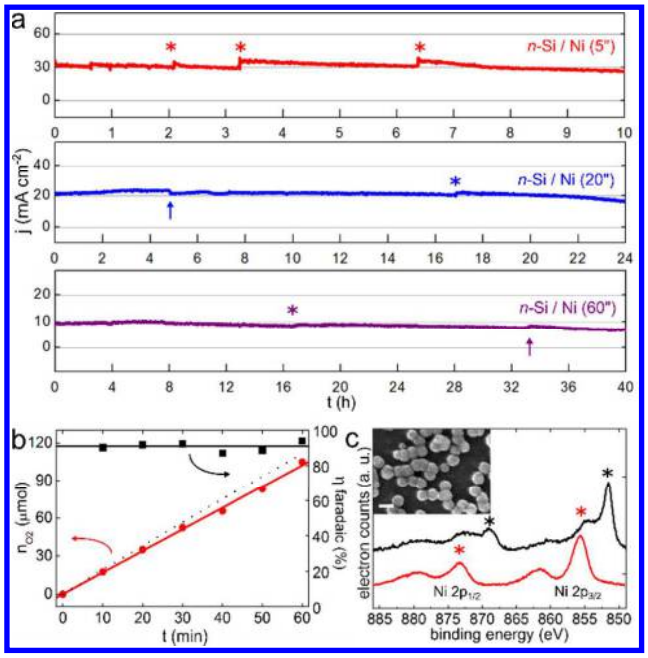

Figure 3. Stability and faradaic efficiency of the photoanodes. a) CAs obtained during prolonged photoelectrolysis in 1 M NaOH under AM 1.5G illumination at +1 V vs SCE for *n*-Si surfaces coated with Ni that was electrodeposited for 5 s (red), 20 s (blue) and 60 s (purple). The asterisks indicate when bubbles were removed from the surface, arrows indicate when the electrolysis was stopped and the photoelectrodes were dried and stored overnight. b) Number of moles of O_2 produced (red disks are experimental data and the red line is a linear fit) during a preparative electrolysis at +1 V vs SCE using a *n*-Si surface coated with Ni for 5 s (see SI for more details). The black dotted line is the theoretical amount of O_2, the black squares and the black line are the faradaic efficiencies and its average value, respectively. c) XPS spectra of the Ni 2p region for the *n*-Si surface coated with Ni for 20 s; after preparation (black line) and after ≈25 h of electrolysis (red line). The black asterisks indicate Ni^0 peaks and the red asterisks indicate Ni

oxides peaks (more information on the spectra is provided in the SI). Inset: SEM picture showing the corresponding surface after electrolysis, the scale bar corresponds to 100 nm.

These data clearly demonstrate that our photoanodes are particularly robust, even if the Ni deposits are not conformal. This is also shown by the fact that they maintained their activity after being stored in air (ambient conditions) overnight when the electrolysis was stopped. Such a stability was unexpected because, in the case of our best-performing photoanodes, most of the Si is in contact with the solution and therefore passivated with a SiO_x layer. X-ray photoelectron spectroscopy (XPS), confirmed the presence of oxygen on the freshly prepared surface and its significant increase after electrolysis (Fig. S13), suggesting that the Si surface is initially covered by a SiO_x layer that grows during the anodic polarization. Therefore, the photocatalytic performances and the stability seem related to the generation of an effective inhomogeneous metal-insulator-semiconductor (MIS) structure (Ni-SiO_x-Si).[8,26] Interestingly, we clearly observe that the stability is enhanced with an increasing amount of Ni, showing that thicker and denser Ni coatings decrease the photocorrosion kinetics by protecting underlying Si from the oxidative solution. However, the stability is increased at the expense of the photocurrent density and photovoltage (Table S2). Like previously reported for electrodeposited discontinuous Co films[26] and evaporated Ni layers behaving as inhomogeneous buried junctions,[28] thicker catalytic layers led, in our case, to weaker light-limited photocurrents and photovoltages.

Gas chromatography (GC) confirmed that the produced gas was O_2. The best photoanode configuration (5 s electrodeposition) was tested by additional electrolyses in a Hoffman cell, which allowed measuring the volume of produced O_2 (see the SI for details). Fig. 3b shows that the photoelectrode produced O_2 at a rate of 4.5 μmol min^{-1} cm^{-2}, which corresponds to a faradaic

efficiency higher than >90 %, this was also confirmed by another set of experiments described in the supporting information (see the SI and Fig. S10). Based on the amount of O_2 produced in Fig. 3b and the number of active Ni sites determined by measuring the charge under the Ni^{3+}/Ni^{2+} wave of the CV (shown in Fig. S11), we calculated a turnover frequency (TOF) of 1.14 $x10^5$ h^{-1} (see supporting information for more details). Most of the electrodeposited Ni was still present on the surface after ≈25 h of electrolysis, as shown by SEM and XPS (Fig. 3c and in Fig. S12), which demonstrates the robustness of the interaction between the Ni NPs and the Si surface.

In conclusion, we have demonstrated that *n*-Si surfaces coated with electrodeposited Ni can be used as efficient photoanodes with faradaic yields >90 % in strongly alkaline pH. The best performances in terms of photovoltage, onset potential and photocurrent density are in the same range than the one reported for more complicated thin layer processes on *n*-Si (table S1) and were obtained for randomly-dispersed Ni NPs, which led to a stability of 10 h at the light-limited photocurrent density (33 mA cm^{-2}). We have shown that stability can be extended to 40 h by increasing the amount of Ni on the surface, which is detrimental to the photovoltage and photocurrent. Moreover, we have demonstrated that Ni coverage can be finely controlled by electrodeposition, which makes it a powerful tool for tuning the photoelectrode activity. These results show that cheap and reliable photoanodes can be simply fabricated without the need of high vacuum techniques. We anticipate that the performances reported here will be soon further improved by employing surface texturing[30] and buried np^+ junctions. Electrodeposition could be beneficially used to improve the electrode design, for instance, by tuning the morphology of the Ni nanocatalysts, additionally, these surfaces may be appealing structures for studying fundamental phenomena taking place at Si-based photoanodes.

ASSOCIATED CONTENT

Supporting Information. The Supporting Information containing the experimental procedure and the supplementary figures and tables is available free of charge on the ACS Publications website.

AUTHOR INFORMATION

gabriel.loget@univ-rennes1.fr

Notes

The authors declare no competing financial interest.

ACKNOWLEDGMENT

This work is partly funded by ANR (project EASi-NANO, ANR-16-CE09-0001-01) and has also been supported by Rennes Métropole (AIS 16C402). Cécile Valter-Potier is acknowledged for the fabrication of the electrochemical cells. Francis Gouttefangeas and Loic Joanny (ScanMAT-CMEBA, Univ. Rennes 1) are acknowledged for SEM imaging.

REFERENCES

(1) Lewis, N. S.; Nocera, D. G. Powering the Planet: Chemical Challenges in Solar Energy Utilization. *Proc. Natl. Acad. Sci.* **2006**, *103*, 15729–15735.

(2) Lewis, N. S. Developing a Scalable Artificial Photosynthesis Technology through Nanomaterials by Design. *Nat. Nanotechnol.* **2016**, *11*, 1010–1019.

(3) Walter, M. G.; Warren, E. L.; McKone, J. R.; Boettcher, S. W.; Mi, Q.; Santori, E. A.; Lewis, N. S. Solar Water Splitting Cells. *Chem. Rev.* **2010**, *110*, 6446–6473.

(4) Fujishima, A.; Honda, K. Electrochemical Photolysis of Water at a Semiconductor

Electrode. *Nature* **1972**, *238*, 37–38.

(5) Prévot, M. S.; Sivula, K. Photoelectrochemical Tandem Cells for Solar Water Splitting. *J. Phys. Chem. C* **2013**, *117*, 17879–17893.

(6) Xiang, C.; Weber, A. Z.; Ardo, S.; Berger, A.; Chen, Y.; Coridan, R.; Fountaine, K. T.; Haussener, S.; Hu, S.; Liu, R.; *et al.* Modeling, Simulation, and Implementation of Solar-Driven Water-Splitting Devices. *Angew. Chem. Int. Ed.* **2016**, *55*, 12974–12988.

(7) Sivula, K.; van de Krol, R. Semiconducting Materials for Photoelectrochemical Energy Conversion. *Nat. Rev. Mater.* **2016**, *1*, 15010.

(8) Sun, K.; Shen, S.; Liang, Y.; Burrows, P. E.; Mao, S. S.; Wang, D. Enabling Silicon for Solar-Fuel Production. *Chem. Rev.* **2014**, *114*, 8662–8719.

(9) Xia, Z.; Zhou, X.; Li, J.; Qu, Y. Protection Strategy for Improved Catalytic Stability of Silicon Photoanodes for Water Oxidation. *Sci. Bull.* **2015**, *60*, 1395–1402.

(10) Hu, S.; Lewis, N. S.; Ager, J. W.; Yang, J.; McKone, J. R.; Strandwitz, N. C. Thin-Film Materials for the Protection of Semiconducting Photoelectrodes in Solar-Fuel Generators. *J. Phys. Chem. C* **2015**, *119*, 24201–24228.

(11) Scheuermann, A. G.; Lawrence, J. P.; Kemp, K. W.; Ito, T.; Walsh, A.; Chidsey, C. E. D.; Hurley, P. K.; McIntyre, P. C. Design Principles for Maximizing Photovoltage in Metal-Oxide-Protected Water-Splitting Photoanodes. *Nat. Mater.* **2016**, *15*, 99–105.

(12) Trotochaud, L.; Ranney, J. K.; Williams, K. N.; Boettcher, S. W. Solution-Cast Metal Oxide Thin Film Electrocatalysts for Oxygen Evolution. *J. Am. Chem. Soc.* **2012**, *134*, 17253–17261.

(13) Hunter, B. M.; Gray, H. B.; Müller, A. M. Earth-Abundant Heterogeneous Water Oxidation Catalysts. *Chem. Rev.* **2016**, *116*, 14120–14136.

(14) Kenney, M. J.; Gong, M.; Li, Y.; Wu, J. Z.; Feng, J.; Lanza, M.; Dai, H. High-Performance Silicon Photoanodes Passivated with Ultrathin Nickel Films for Water Oxidation. *Science* **2013**, *342*, 836–840.

(15) Sun, K.; Pang, X.; Shen, S.; Qian, X.; Cheung, J. S.; Wang, D. Metal Oxide Composite Enabled Nanotextured Si Photoanode for Efficient Solar Driven Water Oxidation. *Nano Lett.* **2013**, *13*, 2064–2072.

(16) Chen, L.; Yang, J.; Klaus, S.; Lee, L. J.; Woods-Robinson, R.; Ma, J.; Lum, Y.; Cooper, J. K.; Toma, F. M.; Wang, L.-W.; *et al.* p-Type Transparent Conducting Oxide/n-Type Semiconductor Heterojunctions for Efficient and Stable Solar Water Oxidation. *J. Am. Chem. Soc.* **2015**, *137*, 9595–9603.

(17) Bae, D.; Mei, B.; Frydendal, R.; Pedersen, T.; Seger, B.; Hansen, O.; Vesborg, P. C. K.; Chorkendorff, I. Back-Illuminated Si-Based Photoanode with Nickel Cobalt Oxide Catalytic Protection Layer. *ChemElectroChem* **2016**, *3*, 1546–1552.

(18) Mei, B.; Permyakova, A. A.; Frydendal, R.; Bae, D.; Pedersen, T.; Malacrida, P.; Hansen, O.; Stephens, I. E. L.; Vesborg, P. C. K.; Seger, B.; *et al.* Iron-Treated NiO as a Highly Transparent p-Type Protection Layer for Efficient Si-Based Photoanodes. *J. Phys. Chem. Lett.* **2014**, *5*, 3456–3461.

(19) Hu, S.; Shaner, M. R.; Beardslee, J. A.; Lichterman, M.; Brunschwig, B. S.; Lewis, N. S. Amorphous TiO_2 Coatings Stabilize Si, GaAs, and GaP Photoanodes for Efficient Water Oxidation. *Science* **2014**, *344*, 1005 LP-1009.

(20) Shaner, M. R.; Hu, S.; Sun, K.; Lewis, N. S. Stabilization of Si Microwire Arrays for Solar-Driven H_2O Oxidation to O_2(g) in 1.0 M KOH(aq) Using Conformal Coatings of Amorphous TiO_2. *Energy Environ. Sci.* **2015**, *8*, 203–207.

(21) Sun, K.; Saadi, F. H.; Lichterman, M. F.; Hale, W. G.; Wang, H.-P.; Zhou, X.; Plymale, N. T.; Omelchenko, S. T.; He, J.-H.; Papadantonakis, K. M.; *et al.* Stable Solar-Driven Oxidation of Water by Semiconducting Photoanodes Protected by Transparent Catalytic Nickel Oxide Films. *Proc. Natl. Acad. Sci. USA* **2015**, *112*, 3612–3617.

(22) Sun, K.; McDowell, M. T.; Nielander, A. C.; Hu, S.; Shaner, M. R.; Yang, F.; Brunschwig, B. S.; Lewis, N. S. Stable Solar-Driven Water Oxidation to O_2(g) by Ni-Oxide-Coated Silicon Photoanodes. *J. Phys. Chem. Lett.* **2015**, *6*, 592–598.

(23) Sun, K.; Park, N.; Sun, Z.; Zhou, J.; Wang, J.; Pang, X.; Shen, S.; Noh, S. Y.; Jing, Y.; Jin, S.; *et al.* Nickel Oxide Functionalized Silicon for Efficient Photo-Oxidation of Water. *Energy Environ. Sci.* **2012**, *5*, 7872–7877.

(24) Sun, K.; Shen, S.; Cheung, J. S.; Pang, X.; Park, N.; Zhou, J.; Hu, Y.; Sun, Z.; Noh, S. Y.; Riley, C. T.; *et al.* Si Photoanode Protected by a Metal Modified ITO Layer with Ultrathin NiO_x for Solar Water Oxidation. *Phys. Chem. Chem. Phys.* **2014**, *16*, 4612–4625.

(25) Reece, S. Y.; Hamel, J. A.; Sung, K.; Jarvi, T. D.; Esswein, A. J.; Pijpers, J. J. H.; Nocera, D. G. Wireless Solar Water Splitting Using Silicon-Based Semiconductors and Earth-Abundant Catalysts. *Science* **2011**, *334*, 645 LP-648.

(26) Hill, J. C.; Landers, A. T.; Switzer, J. A. An Electrodeposited Inhomogeneous Metal-Insulator-Semiconductor Junction for Efficient Photoelectrochemical Water Oxidation. *Nat. Mater.* **2015**, *14*, 1150–1155.

(27) Yu, X.; Yang, P.; Chen, S.; Zhang, M.; Shi, G. NiFe Alloy Protected Silicon Photoanode for Efficient Water Splitting. *Adv. Energy Mater.* **2016**, 1601805.

(28) Laskowski, F. A. L.; Nellist, M. R.; Venkatkarthick, R.; Boettcher, S. W. Junction Behavior of n-Si Photoanodes Protected by Thin Ni Elucidated from Dual Working Electrode

Photoelectrochemistry. *Energy Environ. Sci.* 2017, DOI: 10.1039/c6ee03505a

(29) Medway, S. L.; Lucas, C. A.; Kowal, A.; Nichols, R. J.; Johnson, D. In Situ Studies of the Oxidation of Nickel Electrodes in Alkaline Solution. *J. Electroanal. Chem.* **2006**, *587*, 172–181.

(30) Santinacci, L.; Diouf, M. W.; Barr, M. K. S.; Fabre, B.; Joanny, L.; Gouttefangeas, F.; Loget, G. Protected Light-Trapping Silicon by a Simple Structuring Process for Sunlight-Assisted Water Splitting. *ACS Appl. Mater. Interfaces* **2016**, *8*, 24810–24818.

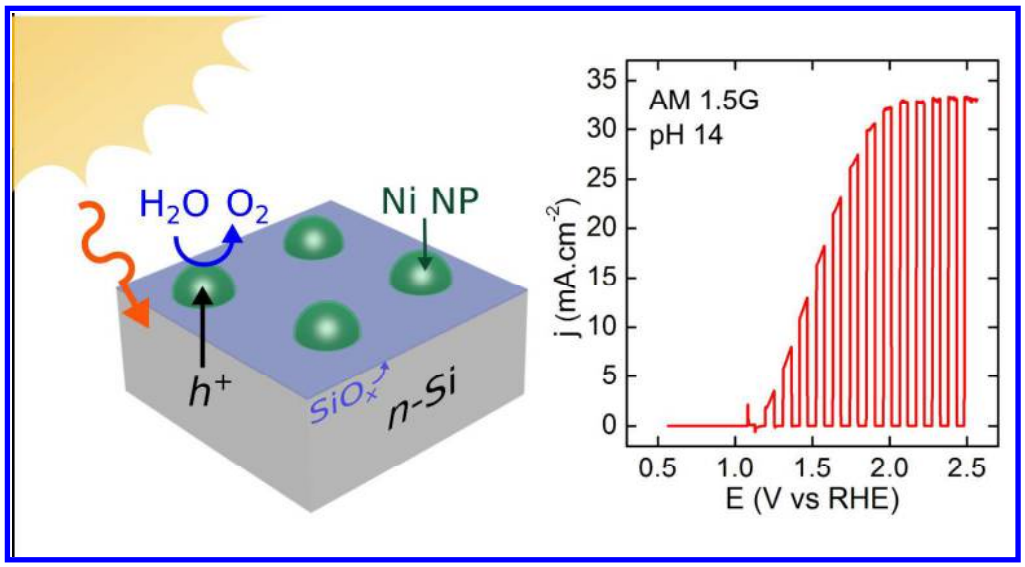

TOC

1286x697mm (72 x 72 DPI)

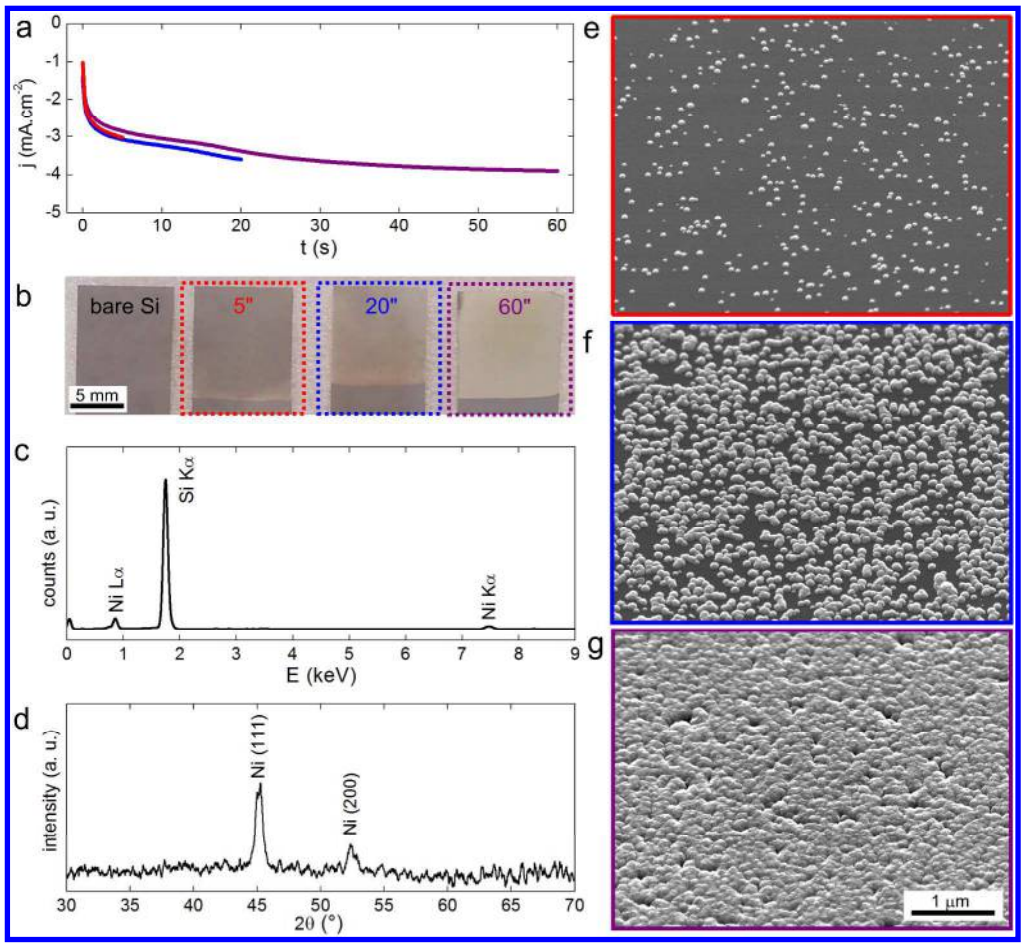

Figure 1. Characterization of the Ni-decorated surfaces. a) Chronoamperograms for Ni electrodeposition on hydrogenated n-Si. b) Photographs of bare and Ni-coated n-Si. c) EDS and d) XRD spectra of Ni-coated n-Si. e-g) SEM pictures showing the Ni deposits on n-Si (the surfaces were tilted by 45°). In these panels, data depicted or framed in red, blue and purple correspond to the surfaces obtained for electrodeposition times of 5 s, 20 s and 60 s, respectively.

1426x1315mm (72 x 72 DPI)

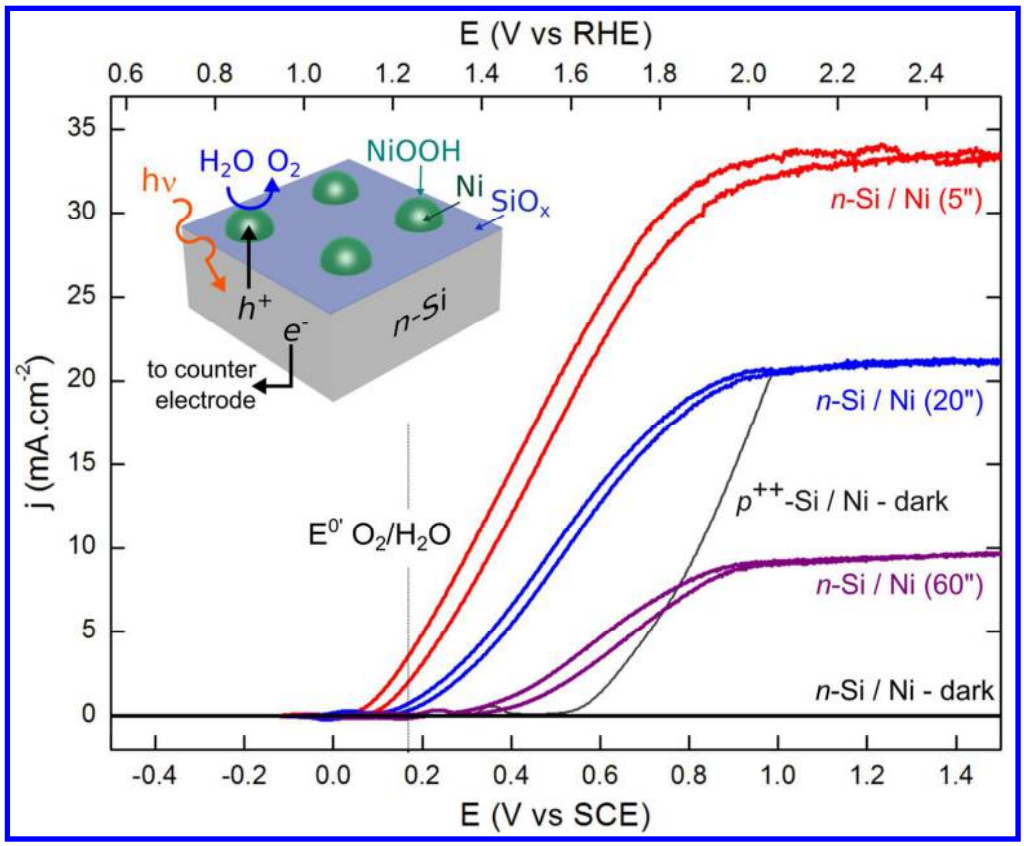

Figure 2. Photoelectrochemical water oxidation. CVs measured in the dark for n-Si decorated with Ni NPs (thick black line) and p++-Si coated with Ni (thin black line) and under illumination (AM 1.5G, 100 mW cm-2) for n-Si coated with Ni for 5 s (red line), 20 s (blue line) and 60 s (purple line); all the curves were recorded in 1 M NaOH at a sweep rate of 20 mV s-1. Inset: scheme of the surface under illumination.

65x54mm (600 x 600 DPI)

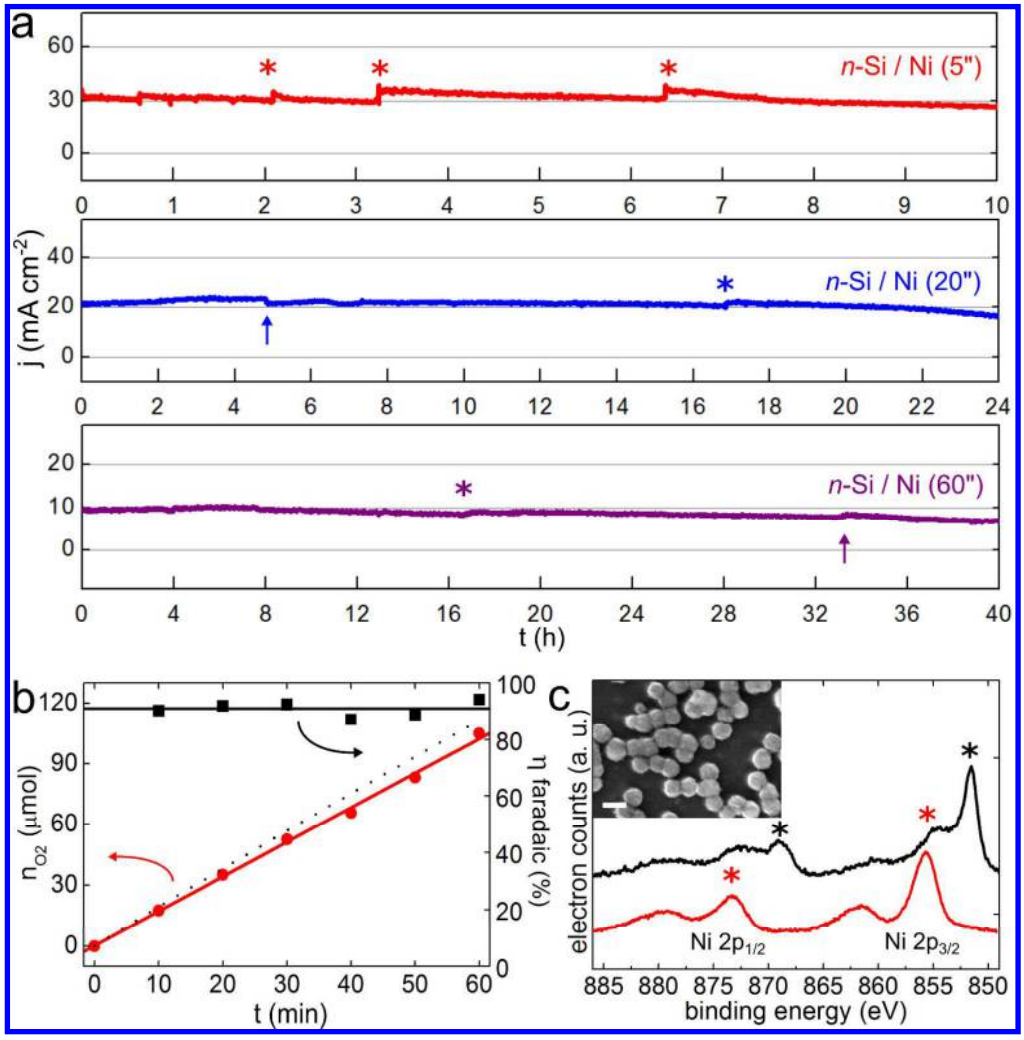

Figure 3. Stability and faradaic efficiency of the photoanodes. a) CAs obtained during prolonged photoelectrolysis in 1 M NaOH under AM 1.5G illumination at +1 V vs SCE for n-Si surfaces coated with Ni that was electrodeposited for 5 s (red), 20 s (blue) and 60 s (purple). The asterisks indicate when bubbles were removed from the surface, arrows indicate when the electrolysis was stopped and the photoelectrodes were dried and stored overnight. b) Number of moles of O2 produced (red disks are experimental data and the red line is a linear fit) during a preparative electrolysis at +1 V vs SCE using a n-Si surface coated with Ni for 5 s (see SI for more details). The black dotted line is the theoretical amount of O2, the black squares and the black line are the faradaic efficiencies and its average value, respectively. c) XPS spectra of the Ni 2p region for the n-Si surface coated with Ni for 20 s; after preparation (black line) and after ≈25 h of electrolysis (red line). The black asterisks indicate Ni0 peaks and the red asterisks indicate Ni oxides peaks (more information on the spectra is provided in the SI). Inset: SEM picture showing the corresponding surface after electrolysis, the scale bar corresponds to 100 nm.

1268x1289mm (72 x 72 DPI)